

www.acsnano.org

Subcellular Targeted Nanohoop for One- and Two-Photon Live Cell Imaging

Terri C. Lovell, Sarah G. Bolton, John P. Kenison, Julia Shangguan, Claire E. Otteson, Fehmi Civitci, Xiaolin Nan,* Michael D. Pluth,* and Ramesh Jasti*



Cite This: ACS Nano 2021, 15, 15285-15293



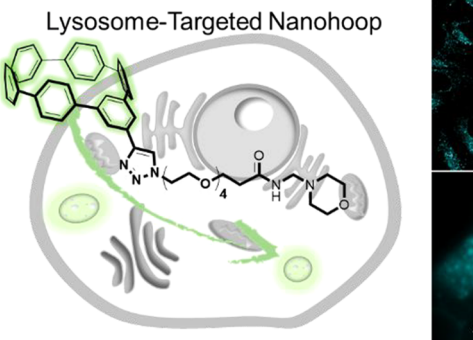
ACCESS

III Metrics & More

Article Recommendations

Supporting Information

ABSTRACT: Fluorophores are powerful tools for interrogating biological systems. Carbon nanotubes (CNTs) have long been attractive materials for biological imaging due to their near-infrared excitation and bright, tunable optical properties. The difficulty in synthesizing and functionalizing these materials with precision, however, has hampered progress in this area. Carbon nanohoops, which are macrocyclic CNT substructures, are carbon nanostructures that possess ideal photophysical characteristics of nanomaterials, while maintaining the precise synthesis of small molecules. However, much work remains to advance the nanohoop class of fluorophores as biological imaging agents. Herein, we report an intracellular targeted nanohoop. This fluorescent nanostructure is noncytotoxic at





concentrations up to 50 μ M, and cellular uptake investigations indicate internalization through endocytic pathways. Additionally, we employ this nanohoop for two-photon fluorescence imaging, demonstrating a high two-photon absorption cross-section (65 GM) and photostability comparable to a commercial probe. This work further motivates continued investigations into carbon nanohoop photophysics and their biological imaging applications.

KEYWORDS: nanohoop, cycloparaphenylene, fluorophore, cell imaging, aromatic molecules

INTRODUCTION

Fluorescence imaging allows for noninvasive observation of biological processes in living systems. A wide variety of fluorophores are available (Figure 1a) including small molecule organic dyes and nanomaterials such as nanoparticles, quantum dots, and carbon nanotubes (CNTs).1-3 Quantum dots are effective imaging agents due to their solubility, brightness, photostability, and tunable emission.^{4,5} However, they are limited by cell impermeability and toxicity to both biological samples and production personnel.^{6,7} CNTs are cellcompatible fluorophores with low toxicity and near-infrared excitation wavelengths. $^{8-10}$ Unfortunately, their optical properties are a direct result of their molecular structure, which cannot be synthesized with atomic precision. 11,12 CNT functionalization, length, type, and purity are extremely difficult to control. 11217 In contrast, small molecule fluorophores permit precise synthetic control and tunability. Modifications of these structures have fueled advances in bioimaging such as improved spatial resolution, deeper tissue penetration, and multiplexing capabilities. 18-20 However, small molecules are not without their pitfalls. Common issues with small molecule fluorophores are water solubility, cytotoxicity, pH sensitivity,²¹ brightness,¹ and photostability.^{22,23} Design

and construction of ideal fluorophores is a formidable challenge and thus continuous effort toward improvement of known scaffolds is underway. Completely new biocompatible optical materials, however, could provide photophysical properties unattainable with traditional small molecule scaffolds.

Recently, a large array of small macrocyclic CNT fragments, often referred to as carbon nanohoops, have become available due to bottom-up synthetic organic methods. Carbon nanohoops possesses ideal characteristics of nanomaterials while having the precise, tunable synthesis of small molecules. In their simplest form, carbon nanohoops are [n]cycloparaphenylenes ([n]CPPs) where "n" phenylene units are bent into a para-linked macrocycle resembling a short CNT slice (Figure 1b, left). Unlike common small molecule fluorophores,

Received: July 17, 2021 Accepted: August 27, 2021 Published: September 2, 2021





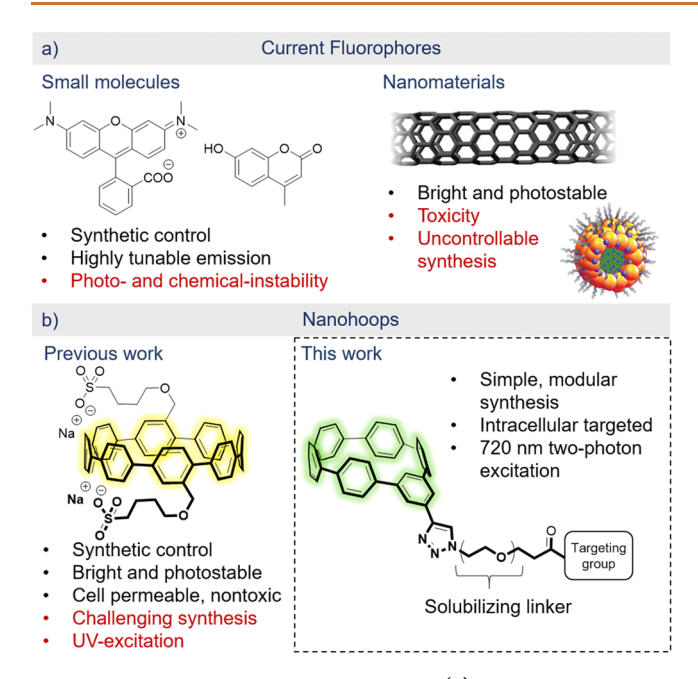


Figure 1. Advantages and challenges with (a) current fluorophore classes used for biological imaging and (b) nanohoops as an emerging class of biological fluorophores.

nanohoops are chemically robust, ^{24–26} and their curvature allows solubility in polar solvents such as dimethyl sulfoxide (DMSO). ^{27,28} The large effective Stokes shifts (110–250 nm) of CPPs result in no spectral overlap between absorbance and emission peaks, allowing full emission collection. This is in stark contrast to xanthene, cyanine, and BODIPY dyes. ¹ Additionally, the controlled nanohoop synthesis permits facile tuning of fluorescence properties. ^{29–33} Recently, it was shown by theory that these materials can be engineered to have near-infrared emissions, further expanding their capabilities. ³¹ These characteristics position nanohoops as promising fluorescent scaffolds for biological applications.

Although carbon nanohoops are rapidly being explored as optical and electronic materials, ^{34–41} studies focused on the their use in biological systems are only beginning to emerge. In 2018, sulfonated [8]CPP (Figure 1b, left) allowed for the initial biological investigations of these materials. The nanohoop retains its brightness in aqueous buffer and was effectively internalized by HeLa cells with minimal toxicity.²⁴ Additionally, a folic acid-functionalized [8]CPP was successfully targeted to cell surface folate receptors. The only other study of these structures in a biological context was conducted by Jiang et al. 42 In this work, the authors demonstrated that [10]CPP can be assembled into nanoscale vesicles that are readily taken up by cells through an energy independent pathway. While these findings demonstrate the potential for CPP use in biological imaging, challenges remain. Building on our prior work, we sought to address key challenges to creating nanohoops for biological imaging.

First, in our initial work, sulfonated [8] CPP (Figure 1b, left) was synthesized through late stage sulfonation. Unfortunately, this route was challenging and low yielding; an improved general solubility approach would make biocompatible nanohoops more accessible. Second, we sought to determine if standard subcellular targeting techniques were amenable to these carbon nanostructures and to determine the nanohoop uptake mechanism. Finally, in previous work, 340 nm

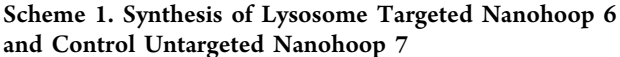
excitation light was used for imaging, but we envisioned that two-photon excitation with near-infrared light would greatly expand the utility of these fluorophores. Herein, we demonstrate nanohoop compatibility with common targeting techniques and present an intracellular lysosome targeted nanohoop. We demonstrate nanohoop utility for two-photon fluorescence (TPF) applications, with comparable brightness to commonly used TPF fluorophores such as fluorescein and rhodamine 6G. This allowed acquisition of bright nanohoop images at low probe concentrations and low doses of near-infrared excitation light. Together, these results showcase the excellent nanohoop performance for biological targeting and imaging.

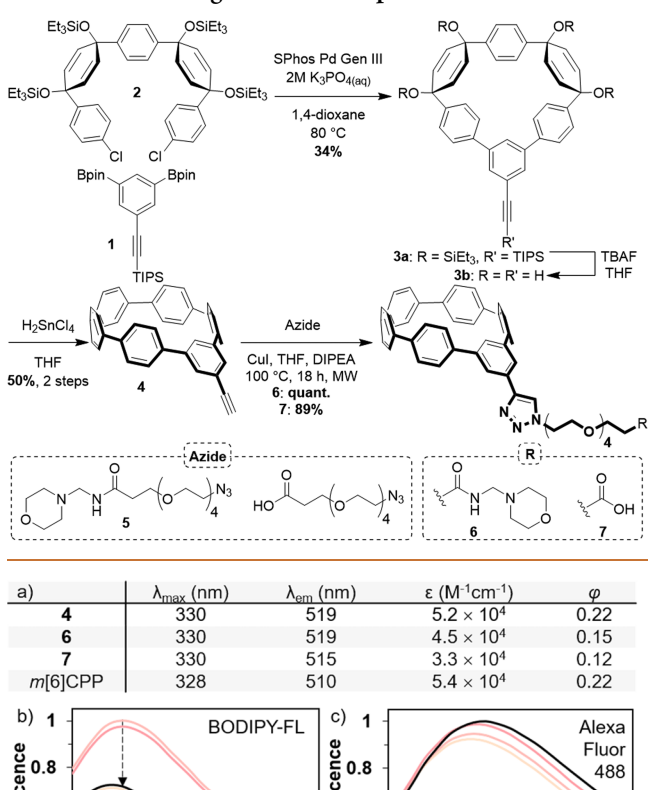
RESULTS AND DISCUSSION

Synthesis. To expand nanohoop generality and accessibility as biocompatible fluorophores, our first goal was to develop a general synthetic strategy allowing nanohoop functionalization with targeting and solubilizing groups. Over the years many different functional groups have been explored to yield biocompatible CPPs.²⁴ A challenge with nanohoop synthesis is the ability to carry functional groups throughout the synthesis, which employs strongly basic and reductive conditions. This limitation necessitates the use of protecting groups, which in turn increases the synthesis length, decreases overall yield, and reduces atom efficiency. Additionally, modifications after nanohoop formation are challenging due to the small quantities of nanohoop typically obtained. We envisioned that azide-alkyne click chemistry could be a suitable method to install both the functionality and solubility needed. Moreover, the click partner can contain a large variety of solubilizing and functional groups, providing a modular synthetic approach to this class of materials. With this concept in mind, we set our sights on a lysosome-targeted nanohoop to evaluate compatibility of these structures with current cellular targeting strategies.

We chose to focus on meta[6]CPP (m[6]CPP) due to its facile synthesis and relatively bright emission. meta[n] CPPs are nanohoops in which one phenylene in the hoop is connected by a meta-linkage as opposed to a para-linkage. Smaller [n]CPPs (n < 7) are nonfluorescent due to symmetry rules. However, inserting a meta-linkage breaks the symmetry allowing fluorescence for all size nanohoops.²⁹ An alkyne was incorporated into m[6]CPP for click-mediated functionalization through macrocyclization of bisboronate 1 and dichloride 2, which can be prepared on the multigram scale (Scheme 1). Deprotection of the silyl protecting groups and mild reductive aromatization afforded 4. The lysosome-targeted nanohoop was prepared through click reaction of nanohoop 4 and azide 5, affording morpholine functionalized nanohoop 6. The morpholine moiety is protonated in the acidic lysosomes, preventing 6 from exiting, thus restricting the fluorophores in the lysosome.⁴⁵ A carboxylic acid analog lacking the targeting group, nanohoop 7, was similarly synthesized as a control compound. Characterization by NMR (¹H and ¹³C), IR, and mass spectrometry confirmed the structural assignment.

Photophysical Characterization. The photophysical properties of 6 and 7 are similar to unfunctionalized m[6]CPP (Figure 2a).²⁹ The absorbance maxima of 4, 6, and 7 are all at 330 nm, compared to 328 nm for m[6]CPP. This main absorption is dominated by HOMO $-1 \rightarrow$ LUMO and HOMO \rightarrow LUMO + 1 transitions.²⁹ The absorption coefficients of 6 (45 000 M⁻¹ cm⁻¹) and 7 (33 000 M⁻¹ cm⁻¹)





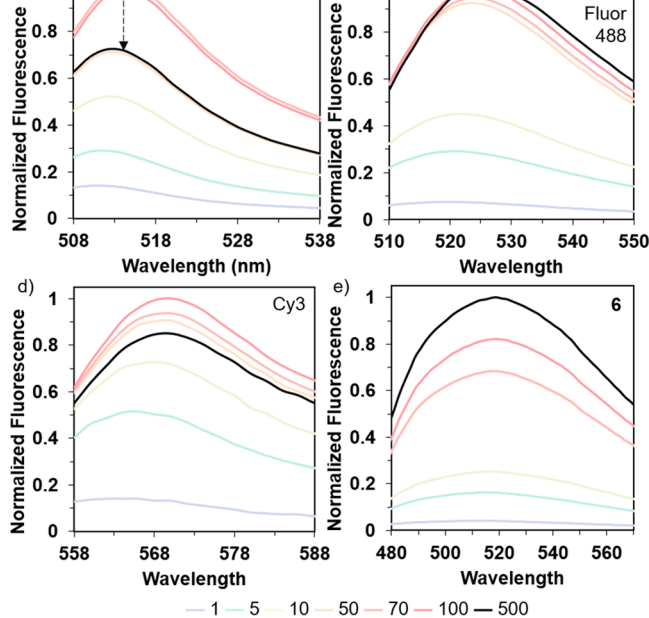


Figure 2. (a) Photophysical properties of 4, 6, and 7 in DMSO and comparison to parent m[6]CPP in CH2Cl2. Fluorescence quenching with increased dye concentrations of (b) BODIPY-FL, (c) Alexa Fluor 488, (d) sulfo-Cy3, and (e) 6 to investigate aggregation induced quenching of planar dyes compared to curved nanohoop 6. All dyes were dissolved in DMSO and diluted in phosphate-buffered saline.

Increasing Concentration (µM)

10

in DMSO are close to that of unfunctionalized m[6]CPP in dichloromethane. A second smaller absorption is observed at 424 nm, corresponding to the HOMO → LUMO transition.²⁹ Nanohoop 6 emission in DMSO peaks at 519 nm, resulting in a 114 nm Stokes shift, which is relatively large for small

molecule fluorophores used in biological imaging. The large Stokes shift arises from structural relaxation in the excited state due to strain. The Stokes shift increases with decreasing nanohoop size resulting from increased strain. This produces greater sp³ hybridization and allows a large decrease in dihedral angles between neighboring phenylenes in the excited state. This results in a large excited state relaxation and, therefore, large Stokes shifts. 46 This large Stokes shift provides complete separation between the excitation and emission, allowing full emission collection. The quantum yield of 6 (0.15) and 7 (0.12) in DMSO are about half that of m[6]CPP in dichloromethane (Figure 2a). This is likely due to functionalization since the quantum yield of 4 in DMSO is the same as the parent m[6]CPP in chloroform.

To compare the nanohoop photophysical properties to other fluorophores, we calculate their brightness, which is defined as the product of the absorption coefficient and quantum yield. Nanohoop 4 has comparable, or higher, brightness than common UV-excitable commercial dyes. Nanohoop 4 has a brightness of 11 440 M⁻¹ cm⁻¹, which is between DAPI nuclear stain (7000 M⁻¹ cm⁻¹) and 7-amino-4-methylcoumarin (AMC, 14 000 M^{-1} cm⁻¹). The 50% quantum yield decrease of 6 and 7 reduces the overall brightness of these nanohoops, but nevertheless, 6 still provides bright one- and two-photon images (vide infra).

We hypothesized that the excellent nanohoop performance as an imaging agent, despite the lower quantum yield, is in part due to the curved structure. As opposed to common flat small molecule fluorophores, the nonplanar nanohoop structure prevents $\pi - \pi$ stacking and should mitigate aggregation induced quenching. Self-quenching is largely problematic when dye molecules are in close proximity, which can result in nonfluorescent dimers or larger aggregates.²

This hypothesis was tested by concentration dependent fluorescence studies of 6 compared to Alexa Fluor 488, BODIPY-FL, and sulfo-Cy3 (Figure 2b-e). BODIPY-FL fluorescence, Figure 2b, shows an initial increase with increasing concentration but begins to decrease at concentrations above 70 μ M. When the Alexa Fluor 488 concentration is increased, the fluorescence shows an initial increase (Figure 2c) and levels off at 100 μ M. Unlike BODIPY-FL, Alexa Fluor dyes are designed to minimize self-quenching through electrostatic repulsion of sulfonic acid groups. Sulfo-Cy3 has fewer sulfonates per carbon atoms than Alexa Fluor 488, so while it is sulfonated, the fluorescence intensity still decreases at high concentrations (500 μ M, Figure 2d). Owing in part to the nonplanar structure of nanohoop 6, introduction of sulfonates is unnecessary for preventing self-quenching. Gratifyingly, the nanohoop fluorescence continually increases without indication of self-quenching even at 500 µM (Figure 2e). Although this is a much higher concentration than that used for cell imaging, when the fluorophore is confined in a specific organelle the local effective concentration is much higher than the 5 μ M of fluorophore introduced. Unfortunately, this is difficult to definitively assess. Lastly, the nonplanar structure should also make 6 less likely to intercalate into DNA, which is a common toxicity mode of polyaromatic hydrocarbon dyes.4

Cytotoxicity, One-Photon Fluorescence Cell Imaging, and Colocalization. To determine the nanohoop utility as a probe for live cell imaging, we first analyzed cytotoxicity. Live HeLa cells were treated with 1, 5, 20, and 50 μ M solutions of 6 or 7 for 1 h. Cell death was measured using CCK-8 cell viability assay. Fluorophores 6 and 7 showed no cytotoxicity even at high concentrations of 50 μ M (Figure 3),

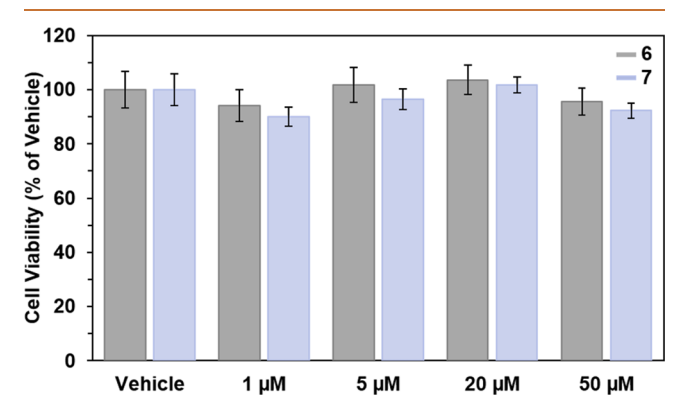


Figure 3. Cytotoxicity studies of 6 and 7 in HeLa cells over 1 h. Neither nanohoop shows significant cytotoxicity even at 50 μ M. Vehicle is 0.5% DMSO.

demonstrating excellent cell-compatibility. This is a significant improvement in cell viability over the previously synthesized nanohoop fluorophore, which showed cytotoxicity at nanohoop concentrations above 10 μ M.

To determine whether nanohoops 6 and 7 are cell permeable, HeLa cells were treated with 5 μ M either 6 or 7 in fetal bovine serum-free Dulbecco's modified eagle medium (DMEM) in a 0.5% DMSO vehicle for 15 min and imaged on a confocal microscope. Where indicated, cells were coincubated with LysoTracker Deep Red or MitoTracker Deep Red. Nanohoops were excited with a 405 nm laser, and commercial Deep Red organelle targeted probes were excited at 633 nm. Despite the moderate quantum yield and brightness of 6 and 7 at 405 nm (HOMO → LUMO transition), bright cell images were still obtained. Nanohoop 6 appeared as sharp puncta localized outside the nucleus (Figure 4a). Co-incubation of LysoTracker Deep Red and 6 show strong colocalization, with a Pearson's coefficient of 0.82. Furthermore, colocalization of 6 and mitochondria-targeted MitoTracker Deep Red is minimal, with a 0.46 Pearson's coefficient (Figure 4c). On the other hand, untargeted 7 appears primarily throughout the cytosol and, to a lesser extent, the nucleus (Figure 4b). This observation is consistent with previous biological CPP reports.^{24,42} The nontargeted 7 did not colocalize with LysoTracker Deep Red as evidenced by a Pearson coefficient of 0.24. This data indicates that the morpholine moiety is responsible for lysosome localization. The nanohoop structure has been altered and controllably targeted to a specific intracellular location. No significant changes in cell morphology were observed upon treatment with the nanohoop. Now the question remains: how does this large, curved, aromatic structure make its way into the cell?

Uptake Studies. Defining the mechanism by which fluorophores are internalized aids in directing design principles and understanding functional group tolerance. The initial expectation was uptake through endocytosis due to the nanohoop size and lipophilic nature. Endocytosis is a process in which cells traffic outside material through the cell membrane and into the cytoplasm using vesicles formed from invagination of the cell membrane. Endocytosis is an active transport process where cells must expend energy to transport materials across the cell membrane. Nanohoop uptake through active transport was tested by incubation of 1 μ M 6 with HeLa

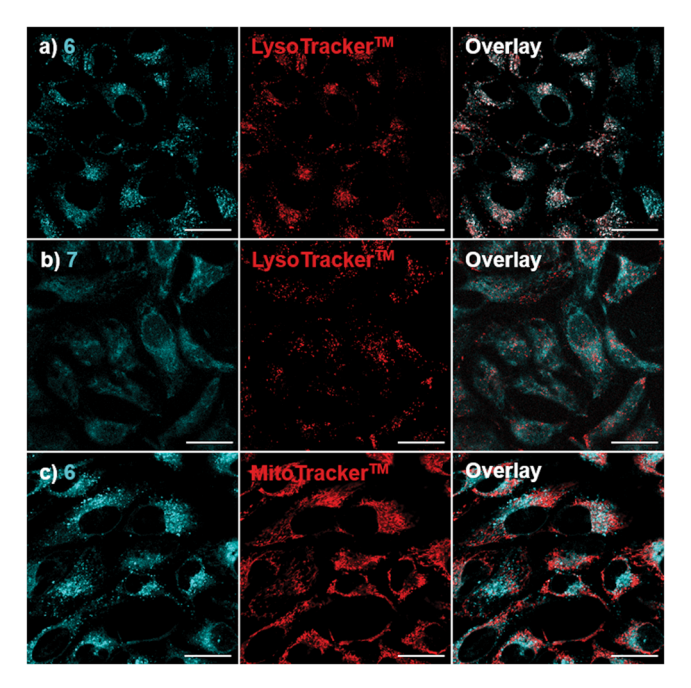


Figure 4. Colocalization of CPPs with commercial probes in HeLa cells. CPPs were coincubated with dyes in a 15 min treatment before imaging via the DAPI channel. LysoTracker Deep Red and MitoTracker Deep Red are visualized in the Cy5 channel. (a) 6 demonstrates a strong trend of colocalization with LysoTracker Deep Red. White areas in the overlay indicate areas of colocalization. Lysosomes are visible as puncta around the nucleus. (b) 7 is diffused throughout the cell with no lysosomal puncta visible nor colocalization with LysoTracker Deep Red, (c) 6 and MitoTracker Deep Red show little colocalization, demonstrating the specific nature of 6 in targeting the lysosome. Scale bars at 30 $\mu \rm m$.

cells for 30 min at either 4, 27, or 37 °C. The uptake was monitored and quantified by fluorescence microscopy. The uptake of 6 was reduced at lower temperatures (Figure 5). A 20% reduction in average intensity per cell is seen between 37 and 27 °C. Incubation at 4 °C reduced nanohoop uptake by 75%, relative to 37 °C. These studies support that nanohoop uptake requires an energy-dependent process, such as endocytosis.⁵⁰

We next evaluated HeLa cell uptake of 6 in the presence of different endocytosis inhibitors. Endocytosis can proceed through several different pathways, including clathrin-mediated, caveolae-mediated, and macripinocytosis.⁴⁸ Uptake inhibitors were used to investigate which processes enabled cellular uptake of 6. Chlorpromazine (CPZ), filipin (FIL), and amiloride were used to inhibit clathrin-mediated, caveolaemediated, and macropinocytotic endocytosis pathways, respectively. Alexa Fluor 488-transferrin (clathrin-mediated), BODIPY-lactosylceramide (caveolae-mediated), and FITCdextran (macropinocytosis) were used as fluorescent controls (Figure S3).50,51 HeLa cells were treated with the inhibitors for 30 min, followed by 15 min incubation with 5 μ M 6. Reduced uptake was observed in all cases, with the largest reduction in clathrin-mediated endocytosis inhibition (Figure 6). The morpholine group on 6 could encourage this uptake method as lysosome-targeting morpholine groups have been shown to enhance lysosomal endocytosis rates. 52-54 However, further studies are needed to elucidate the specific uptake mechanisms further.

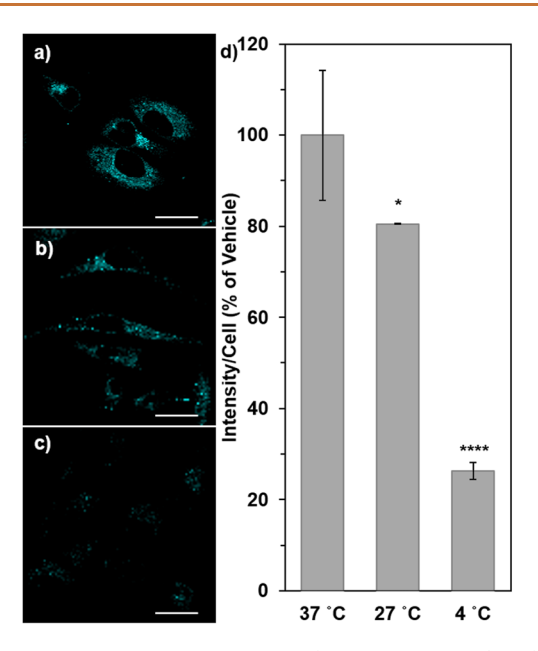


Figure 5. HeLa cell uptake of 1 μ M 6 (30 min treatment) at (a) 37, (b) 27, and (c) 4 °C to (d) quantify cell fluorescence relative to the 37 °C condition. Uptake is slightly inhibited at 27 °C and strongly hindered at 4 °C incubation, demonstrating an energy dependent uptake. Scale bars are at 30 μ m.

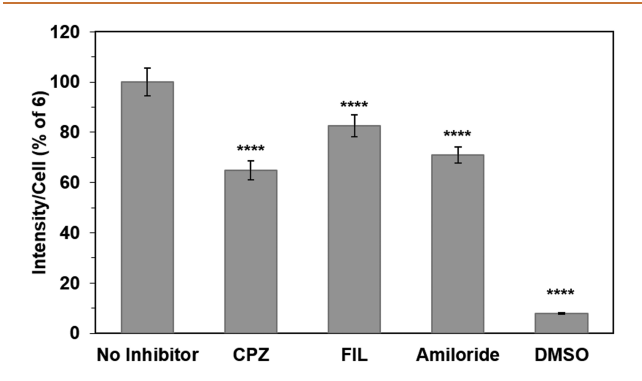


Figure 6. Cell uptake of 6 in the presence of endocytosis inhibitors to investigate endocytic uptake mechanism. All inhibitors caused significant disruption in hoop uptake, with the most significant being chlorpromazine, implicating multiple modes of endocytosis.

Two-Photon Fluorescence Imaging and Characterization. Having established the use of **6** for lysosomal targeting and imaging, we next turned our attention to two-photon fluorescence (TPF) imaging. TPF has emerged as a superior modality for biomedical research due to its intrinsic optical sectioning, high spatial resolution, and near-infrared sample-friendly light source. However, many one-photon fluorescent probes are not compatible with TPF imaging. So

Using a custom built TPF system, the two-photon spectral response and absorption cross-section of **6** in DMSO (250 nM) was analyzed. The excitation wavelength range used is between 705 and 800 nm (Figure 7a). Nanohoop **6** has a peak TPF response at 720 nm, followed by a second peak at 760 nm. The TPF spectra of rhodamine 6G (Figure S4) was measured and compared with literature reports, validating the accuracy of our approach. Using rhodamine 6G as a standard, the TPF absorption cross-section of **6** was determined to be 65 GM at 720 nm. TPF fluorophores such as

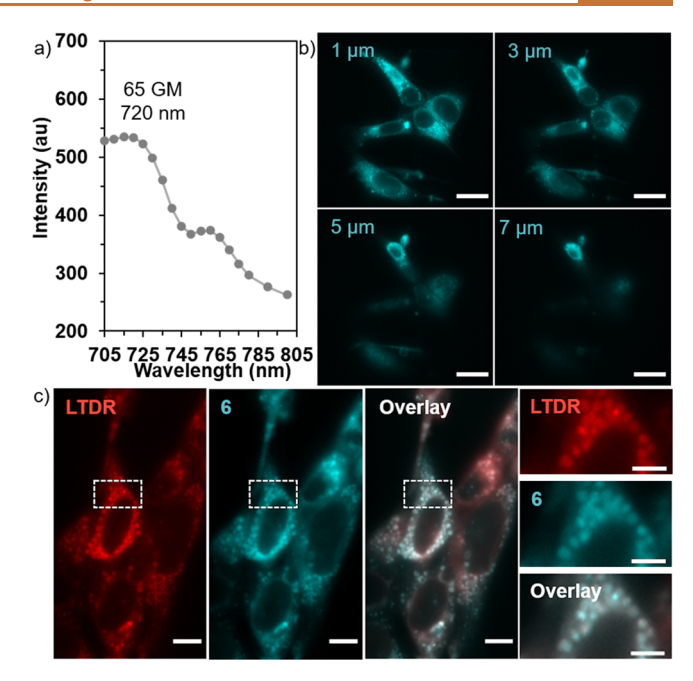


Figure 7. (a) Two-photon excitation spectrum of 250 nM 6 from 680–800 nm measured in DMSO. TPF cross-sections were calculated using a rhodamine 6G reference. (b) TPF images of U2OS cells treated with 6 and acquired at 1 s/frame. Images were taken at a series of focal positions, starting 1 μ m above the coverglass (first panel) and moving up (subsequent panels). See also Supplementary Movie 1. Scale bar 20 μ m. (c) Two-color TPF image of U2OS cells coincubated with 60 nM LysoTracker Deep Red and 60 nM 6. The overlaid image is shown as the third panel. Right panels show the zoom-in views of boxed regions in the left images. Scale bars 20 μ m left panels, and 5 μ m in right zoom-in panels.

fluorescein and rhodamine 6G, which sections between 20–200 GM. This result is very promising as no structural optimizations have been done on the nanohoop scaffold to improve TPF performance. Addition of donor and/or acceptor units to the nanohoop could realize structures with large dipole moments producing superior TPF fluorophores. Further theoretical and experimental studies are required to fully understand the influence of size and symmetry on the multiphoton photophysics of nanohoops.

Next, we examined the TPF of 6 in U2OS cells. TPF images showed endocytosed 6 as well resolved puncta with a high signal to background ratio. U2OS cells were incubated with 60 nM 6 and excited at 720 nm. An excitation power of 100 mW (line scan, equivalent to 1 mW in a point scanning configuration), and a 1 frame/s image acquisition rate were used (Figure 7b). The intrinsic optical sectioning capability of TPF allows whole cell 3D imaging with high resolution by progressively imaging a range of axial positions (Figure 7b and Supplementary Movie 1). Consistent with results from onephoton imaging, 6 and LysoTracker Deep Red (820 nm excitation) signals largely overlap as puncta in the cytosol (Figure 7c, main panel and zoom-in views). In addition to good TPF signal and cellular targeting, we also observed good photostability of 6 at the same excitation power levels (100 mW), allowing continuous imaging for >200 s before noticeable photobleaching (Figure S5). Moreover, 6 only shows a 10% decrease after 5 min of constant illumination at 720 nm and 100 mW, whereas LysoTracker Deep Red decreased by twice that (820 nm, 100 mW). Nanohoop 6

photobleaches faster at higher laser intensities of 200 or 300 mW, but these powers are typically higher than those used for live cell imaging. The change in photobleaching rate is consistent with the nonlinear nature of TPF-induced photobleaching. These results demonstrate excellent performance of 6 as a TPF fluorophore. We anticipate that 6, and potentially many other nanohoops, may deliver even better TPF performance and find broad applications in biological imaging.

CONCLUSIONS

In summary, we synthesized and characterized a nanohoopbased organelle targeted fluorescent probe. Morpholine is used to target the lysosome with high selectivity and was compared with the commercial dye LysoTracker Deep Red. The synthetic methods described in this work allows access to many biocompatible nanohoop structures previously unattainable. The synthesis allows functionalization with an unlimited number of linkers with varying functionality. Additionally, this linker serves to impart functionality as well as solubility, tackling two challenges simultaneously. The synthesized nanohoop fluorophore is noncytotoxic even at 50 µM and cellular uptake mechanistic studies indicate fluorophore uptake occurs through endocytic pathways. Furthermore, we describe the use of nanohoops for two-photon fluorescence imaging, which demonstrates a high two-photon absorption crosssection (65 GM) and photostability comparable to commercial probes. The m[6]CPP scaffold chosen for this initial feasibility work is one of the dimmest nanohoops available, yet produces bright cell images. Therefore, the larger brighter nanohoops available may significantly outperform commercial fluorophores in their emission range. Likewise, the nanohoop structure can be modified to increase the TPF cross-section.

This carbon-based curved molecular structure is unlike other fluorophores used for cellular imaging, offering optical properties unlike any other small molecule fluorophore class. Furthermore, nanohoops are poised for multiplexed and multimodal imaging, making them an intriguing scaffold for fluorophore development. Lastly, the cavity of the nanohoop holds prospect for interesting biologically relevant host—guest applications. As synthetic methods improve and even more carbon nanohoops and nanobelts become available, the promise of precision nanoscience in biology is an exciting one.

METHODS

Materials and Characterization. All reagents used were obtained commercially unless otherwise noted in the Supporting Information. ¹H NMR spectra were recorded at 500 or 600 MHz on a Bruker Advance-III-HD NMR spectrometer. ¹³C NMR spectra were recorded at 150 or 126 MHz on a Bruker Advance-III-HD NMR spectrometer. All ¹H NMR spectra were taken in CDCl₃ (referenced to TMS, δ 0.00 ppm). ¹³C NMR spectra were taken in CDCl₃ (referenced to chloroform, δ 77.16 ppm). Mass spectra were obtained using ASAP. Absorbance and fluorescence spectra were taken with Tecan Spark in a Nunc 96-well plate. Fluorescent quantum yield of 4 was measured in dichloromethane at room temperature using a Hamamatsu absolute PL quantum yield measurement system. Fluorescent quantum yield of 6 and 7 were measured in a 1 cm Quartz cuvette with dimethyl sulfoxide (refractive index 1.479) at room temperature as described by Jobin Yvon Horiba with anthracene (ethanol, refractive index 1.361) and quinine sulfate (0.1 M H₂SO₄, refractive index 1.332) as standards using an Agilent Cary 100 UVvis spectrometer and a Horiba Jobin Yvon Fluoromax-4 Fluorimeter.

Further characterization details are found in the Supporting Information.

Cell Culture. HeLa cells (ATCC CCL-2) were cultured in high glucose Dulbecco's modified Eagle's medium (DMEM) supplemented with 10% premium grade fetal bovine serum (FBS) and 1% penicillin/streptomycin (PS) at 37 °C under 5% CO $_2$. HeLa cells were then plated on poly-D-lysine coated glass-bottom imaging dishes (MatTek) at 1×10^5 cells/dish and incubated at 37 °C under 5% CO $_2$ overnight before performing experiments. Cytotoxicity, colocalization, and uptake study details are found in section 3 of the Supporting Information.

U2OS cells (ATCC HTB-96) were maintained in DMEM supplemented with 10% FBS at 37 $^{\circ}\text{C}$ under 5% CO $_2$. Cells were plated on Lab-Tek II eight-well chambered coverglasses (Thermo-Fisher, 155360) and grown 24–36 h in 10% FBS DMEM at 37 $^{\circ}\text{C}$ under 5% CO $_2$. Prior to imaging, cells were washed 2X with FBS-free DMEM.

Microscopy. One-photon fluorescence imaging was performed on a Zeiss LSM 880 confocal microscope in FluoroBrite DMEM (Gibco). Two-photon fluorescence (TPF) imaging and measurements were performed on a custom microscopy setup built upon a Nikon $Ti-\bar{U}$ inverted microscope frame, using an Insight DeepSee laser (Spectra Physics, CA) as the light source. The Insight produces ~120 fs pulses at a repetition rate of 80 MHz, with the wavelength tunable from 680 to 1300 nm. For TPF imaging of cells, an excitation beam from the Insight was expanded and passed through a cylindrical lens (f = 100 mm) positioned at the entrance of a resonant galvanometer beam scanner (with a resonant frequency at 8 kHz). A 654 nm short pass dichroic (Semrock FF654-SDi01-25 × 36; center cutoff wavelength ~652 nm) was used for 6 with a 720 nm excitation wavelength while an 825 nm short pass dichroic (Semrock FF825-SDi01-25 × 36; center cutoff wavelength at 815 nm) was used for LysoTracker Deep Red stained samples which were excited with 820 nm. Both dichroic mirrors directed the beam to a 60× oil immersion objective, resulting in a line scanning pattern focused in the other dimension perpendicular to the line. The line was then resonantly swept in the direction perpendicular to its long axis to generate images of the field of view (FOV). The total laser power used for TPF imaging was around 100 mW, which is equivalent to ~ 1 mW in a focused, point-scanning system. Fluorescence emission is collected through the same objective and detected on an EMCCD camera. A 708/75 nm band-pass filter was used to filter LysoTracker Deep Red emission while two short pass emission filters (with cutoff wavelengths at 650 and 665 nm) were used for 6. For colabeled samples, an additional 520/35 nm band-pass filter was used to isolate 6 from LysoTracker Deep Red. Details and equations used to calculate the two-photon cross-section are found in section 4 of the Supporting Information.

ASSOCIATED CONTENT

Supporting Information

The Supporting Information is available free of charge at https://pubs.acs.org/doi/10.1021/acsnano.1c06070.

General experimental methods, synthetic procedures, structural and photophysical characterization, and detailed imaging procedures (PDF)
Supplemental Movie 1 (MP4)

AUTHOR INFORMATION

Corresponding Authors

Ramesh Jasti — Department of Chemistry & Biochemistry, Materials Science Institute, Knight Campus for Accelerating Scientific Impact, University of Oregon, Eugene, Oregon 97403, United States; orcid.org/0000-0002-8606-6339; Email: rjasti@uoregon.edu

Xiaolin Nan – Knight Cancer Early Detection Advanced Research Center, Oregon Health and Science University, Portland, Oregon 97201, United States; Department of Biomedical Engineering, Oregon Health and Science University, Portland, Oregon 97201, United States; orcid.org/0000-0002-0597-0255; Email: nan@ohsu.edu

Michael D. Pluth – Department of Chemistry & Biochemistry, Materials Science Institute, Knight Campus for Accelerating Scientific Impact, University of Oregon, Eugene, Oregon 97403, United States; ● orcid.org/0000-0003-3604-653X; Email: pluth@uoregon.edu

Authors

- Terri C. Lovell Department of Chemistry & Biochemistry, Materials Science Institute, Knight Campus for Accelerating Scientific Impact, University of Oregon, Eugene, Oregon 97403, United States; Present Address: T.C.L.: Department of Chemistry, McGill University, Montreal, Quebec, Canada H3A 0B8; orcid.org/0000-0003-1722-584X
- Sarah G. Bolton Department of Chemistry & Biochemistry, Materials Science Institute, Knight Campus for Accelerating Scientific Impact, University of Oregon, Eugene, Oregon 97403, United States
- John P. Kenison Knight Cancer Early Detection Advanced Research Center, Oregon Health and Science University, Portland, Oregon 97201, United States; Present Address: J.P.K.: KLA-Tencor, Hillsboro, Oregon, USA 97006.
- Julia Shangguan Department of Biomedical Engineering, Oregon Health and Science University, Portland, Oregon 97201, United States
- Claire E. Otteson Department of Chemistry & Biochemistry, Materials Science Institute, Knight Campus for Accelerating Scientific Impact, University of Oregon, Eugene, Oregon 97403, United States; orcid.org/0000-0002-0095-6729
- Fehmi Civitci Knight Cancer Early Detection Advanced Research Center, Oregon Health and Science University, Portland, Oregon 97201, United States

Complete contact information is available at: https://pubs.acs.org/10.1021/acsnano.1c06070

Notes

The authors declare no competing financial interest.

ACKNOWLEDGMENTS

Financial support was provided by the National Science Foundation (NSF) grant number CHE-1800586 (RJ), National Institutes of Health (NIH) grant numbers R01GM113030 (MDP), T32GM007759 (SGB), and R01GM132322 (XN), as well as the OHSU-UO Presidents' Collaboration Fund (RJ and XN). We would like to acknowledge Dr. Yu Zhao and Dr. Carey Phelps for their initial efforts on the project. We thank Dr. Bruce Branchaud (OHSU and UO) for helpful discussions, Tavis Price for assistance with mass spectrometry characterization, Dr. Kai Tao for sample preparation assistance, and Dr. Stefanie Kaech Petrie and Crystal Chaw for technical assistance at the OHSU advanced light microscopy core. J.P,K., F.C., and X.N. are members of and supported by the Knight Cancer Early Detection Advanced Research Center at OHSU.

REFERENCES

- (1) Lavis, L. D.; Raines, R. T. Bright Ideas for Chemical Biology. ACS Chem. Biol. 2008, 3, 142-155.
- (2) Mcquade, D. T.; Pullen, A. E.; Swager, T. M. Conjugated Polymer-Based Chemical Sensors. *Chem. Rev.* **2000**, *100*, 2537–2574.
- (3) Hong, G.; Diao, S.; Antaris, A. L.; Dai, H. Carbon Nanomaterials for Biological Imaging and Nanomedicinal Therapy. *Chem. Rev.* **2015**, 115, 10816–10906.
- (4) Chan, W. C. W.; Nie, S. Quantum Dot Bioconjugates for Ultrasensitive Nonisotopic Detection. *Science* **1998**, *281*, 2016–2018.
- (5) Bruchez, M.; Moronne, M.; Gin, P.; Weiss, S.; Alivisatos, A. P. Semiconductor Nanocrystals as Fluorescent Biological Labels. *Science* **1998**, 281, 2013–2016.
- (6) Bradburne, C. E.; Delehanty, J. B.; Boeneman Gemmill, K.; Mei, B. C.; Mattoussi, H.; Susumu, K.; Blanco-Canosa, J. B.; Dawson, P. E.; Medintz, I. L. Cytotoxicity of Quantum Dots Used for *in Vitro* Cellular Labeling: Role of QD Surface Ligand, Delivery Modality, Cell Type, and Direct Comparison to Organic Fluorophores. *Bioconjugate Chem.* 2013, 24, 1570–1583.
- (7) Derfus, A. M.; Chan, W. C. W.; Bhatia, S. N. Intracellular Delivery of Quantum Dots for Live Cell Labeling and Organelle Tracking. *Adv. Mater.* **2004**, *16*, 961–966.
- (8) Panwar, N.; Soehartono, A. M.; Chan, K. K.; Zeng, S.; Xu, G.; Qu, J.; Coquet, P.; Yong, K. T.; Chen, X. Nanocarbons for Biology and Medicine: Sensing, Imaging, and Drug Delivery. *Chem. Rev.* **2019**, 119, 9559–9656.
- (9) Zhu, S.; Yang, Q.; Antaris, A. L.; Yue, J.; Ma, Z.; Wang, H.; Huang, W.; Wan, H.; Wang, J.; Diao, S.; Zhang, B.; Li, X.; Zhong, Y.; Yu, K.; Hong, G.; Luo, J.; Liang, Y.; Dai, H. Molecular Imaging of Biological Systems with a Clickable Dye in the Broad 800-to 1,700-Nm Near-Infrared Window. *Proc. Natl. Acad. Sci. U. S. A.* **2017**, 114, 962–967.
- (10) Wang, H.; Wang, Z.; Ye, M.; Zong, S.; Li, M.; Chen, P.; Ma, X.; Cui, Y. Optically Encoded Nanoprobes Using Single Walled Carbon Nanotube as the Building Scaffold for Magnetic Field Guided Cell Imaging. *Talanta* **2014**, *119*, 144–150.
- (11) Ohfuchi, M.; Miyamoto, Y. Optical Properties of Oxidized Single-Wall Carbon Nanotubes. *Carbon* **2017**, *114*, 418–423.
- (12) Ghosh, S.; Bachilo, S. M.; Weisman, R. B. Advanced Sorting of Single-Walled Carbon Nanotubes by Nonlinear Density-Gradient Ultracentrifugation. *Nat. Nanotechnol.* **2010**, *5*, 443–450.
- (13) Jorio, A.; Dresselhaus, G.; Dresselhaus, M. S. Carbon Nanotubes; Springer: Heidelberg, 2008.
- (14) Yang, F.; Wang, X.; Zhang, D.; Yang, J.; Luo, D.; Xu, Z.; Wei, J.; Wang, J. Q.; Xu, Z.; Peng, F.; Li, X.; Li, R.; Li, Y.; Li, M.; Bai, X.; Ding, F.; Li, Y. Chirality-Specific Growth of Single-Walled Carbon Nanotubes on Solid Alloy Catalysts. *Nature* **2014**, *510*, 522–524.
- (15) He, M.; Jiang, H.; Liu, B.; Fedotov, P. V.; Chernov, A. I.; Obraztsova, E. D.; Cavalca, F.; Wagner, J. B.; Hansen, T. W.; Anoshkin, I. V.; Obraztsova, E. A.; Belkin, A. V.; Sairanen, E.; Nasibulin, A. G.; Lehtonen, J.; Kauppinen, E. I. Chiral-Selective Growth of Single-Walled Carbon Nanotubes on Lattice-Mismatched Epitaxial Cobalt Nanoparticles. *Sci. Rep.* **2013**, DOI: 10.1038/srep01460.
- (16) Sanchez-Valencia, J. R.; Dienel, T.; Gröning, O.; Shorubalko, I.; Mueller, A.; Jansen, M.; Amsharov, K.; Ruffieux, P.; Fasel, R. Controlled Synthesis of Single-Chirality Carbon Nanotubes. *Nature* **2014**, *512*, 61–64.
- (17) Hersam, M. C. Progress towards Monodisperse Single-Walled Carbon Nanotubes. *Nat. Nanotechnol.* **2008**, *3*, 387–394.
- (18) Cosco, E. D.; Spearman, A. L.; Ramakrishnan, S.; Lingg, J. G. P.; Saccomano, M.; Pengshung, M.; Arús, B. A.; Wong, K. C. Y.; Glasl, S.; Ntziachristos, V.; Warmer, M.; McLaughlin, R. R.; Bruns, O. T.; Sletten, E. M. Shortwave Infrared Polymethine Fluorophores Matched to Excitation Lasers Enable Non-Invasive, Multicolour *in Vivo* Imaging in Real Time. *Nat. Chem.* **2020**, *12*, 1123–1130.
- (19) Michie, M. S.; Götz, R.; Franke, C.; Bowler, M.; Kumari, N.; Magidson, V.; Levitus, M.; Loncarek, J.; Sauer, M.; Schnermann, M. J.

- Cyanine Conformational Restraint in the Far-Red Range. J. Am. Chem. Soc. 2017, 139, 12406–12409.
- (20) Grimm, J. B.; English, B. P.; Chen, J.; Slaughter, J. P.; Zhang, Z.; Revyakin, A.; Patel, R.; Macklin, J. J.; Normanno, D.; Singer, R. H.; Lionnet, T.; Lavis, L. D. A General Method to Improve Fluorophores for Live-Cell and Single-Molecule Microscopy. *Nat. Methods* **2015**, 12, 244–250.
- (21) Lavis, L. D.; Rutkoski, T. J.; Raines, R. T. Tuning the PKa of Fluorescein to Optimize Binding Assays. *Anal. Chem.* **200**7, 79, 6775–6782.
- (22) Johnson, I. D. Practical Considerations in the Selection and Application of Fluorescent Probes. In *Handbook of Biological Confocal Microscopy*, Third ed.; Pawley, J. B., Ed.; Springer US: Boston, MA, 2006; pp 353–367.
- (23) Dempsey, G. T.; Vaughan, J. C.; Chen, K. H.; Bates, M.; Zhuang, X. Evaluation of Fluorophores for Optimal Performance in Localization-Based Super-Resolution Imaging. *Nat. Methods* **2011**, *8*, 1027–1036.
- (24) White, B. M.; Zhao, Y.; Kawashima, T. E.; Branchaud, B. P.; Pluth, M. D.; Jasti, R. Expanding the Chemical Space of Biocompatible Fluorophores: Nanohoops in Cells. *ACS Cent. Sci.* **2018**, *4*, 1173–1178.
- (25) Cheung, K. Y.; Gui, S.; Deng, C.; Liang, H.; Xia, Z.; Liu, Z.; Chi, L.; Miao, Q. Synthesis of Armchair and Chiral Carbon Nanobelts. *Chem.* **2019**, *5*, 838–847.
- (26) Kayahara, E.; Qu, R.; Yamago, S. Bromination of Cycloparaphenylenes: Strain-Induced Site-Selective Bis-Addition and Its Application for Late-Stage Functionalization. *Angew. Chem., Int. Ed.* **2017**, *56*, 10428–10432.
- (27) Li, P.; Sisto, T. J.; Darzi, E. R.; Jasti, R. The Effects of Cyclic Conjugation and Bending on the Optoelectronic Properties of Paraphenylenes. *Org. Lett.* **2014**, *16*, 182–185.
- (28) Meerholz, K.; Heinze, J. Electrochemical Solution and Solid-State Investigations on Conjugated Oligomers and Polymers of the α -Thiophene and the p-Phenylene Series. *Electrochim. Acta* **1996**, 41, 1839–1854.
- (29) Lovell, T. C.; Colwell, C. E.; Zakharov, L. N.; Jasti, R. Symmetry Breaking and the Turn-on Fluorescence of Small, Highly Strained Carbon Nanohoops. *Chem. Sci.* **2019**, *10*, 3786–3790.
- (30) Lovell, T. C.; Garrison, Z. R.; Jasti, R. Synthesis, Characterization and Computational Investigation of Bright Orange-Emitting Benzothiadiazole [10]Cycloparaphenylene. *Angew. Chem., Int. Ed.* **2020**, 59, 14363.
- (31) Lovell, T. C.; Fosnacht, K. G.; Colwell, C. E.; Jasti, R. Effect of Curvature and Placement of Donor and Acceptor Units in Cycloparaphenylenes: A Computational Study. *Chem. Sci.* **2020**, *11* (11), 12029–12035.
- (32) Qiu, Z.; Tang, C.; Wang, X.; Ju, Y.; Chu, K.; Deng, Z.; Hou, H.; Liu, Y.; Tan, Y. Tetra-Benzothiadiazole-Based [12]-Cycloparaphenylene with Bright Emission and Its Supramolecular Assembly. *Angew. Chem., Int. Ed.* **2020**, *59*, 20868–20872.
- (33) Iwamoto, T.; Watanabe, Y.; Sakamoto, Y.; Suzuki, T.; Yamago, S. Selective and Random Syntheses of [n]Cycloparaphenylenes (n = 8–13) and Size Dependence of Their Electronic Properties. *J. Am. Chem. Soc.* **2011**, *133*, 8354–8361.
- (34) Leonhardt, E. J.; Jasti, R. Emerging Applications of Carbon Nanohoops. *Nat. Rev. Chem.* **2019**, *3*, 672–686.
- (35) Kayahara, E.; Sun, L.; Onishi, H.; Suzuki, K.; Fukushima, T.; Sawada, A.; Kaji, H.; Yamago, S. Gram-Scale Syntheses and Conductivities of [10]Cycloparaphenylene and Its Tetraalkoxy Derivatives. J. Am. Chem. Soc. 2017, 139, 18480–18483.
- (36) Xu, Y.; Wang, B.; Kaur, R.; Minameyer, M. B.; Bothe, M.; Drewello, T.; Guldi, D. M.; von Delius, M. A Supramolecular [10]CPP Junction Enables Efficient Electron Transfer in Modular Porphyrin−[10]CPP⊃Fullerene Complexes. *Angew. Chem., Int. Ed.* **2018**, *57*, 11549−11553.
- (37) Huang, Q.; Zhuang, G.; Jia, H.; Qian, M.; Cui, S.; Yang, S.; Du, P. Photoconductive Curved-Nanographene/Fullerene Supramolecular Heterojunctions. *Angew. Chem., Int. Ed.* **2019**, *58*, 6244–6249.

- (38) Van Raden, J. M.; White, B. M.; Zakharov, L. N.; Jasti, R. Nanohoop Rotaxanes from Active Metal Template Syntheses and Their Potential in Sensing Applications. *Angew. Chem., Int. Ed.* **2019**, *58*, 7341–7345.
- (39) Leonhardt, E. J.; Van Raden, J. M.; Miller, D.; Zakharov, L. N.; Alemán, B.; Jasti, R. A Bottom-Up Approach to Solution-Processed, Atomically Precise Graphitic Cylinders on Graphite. *Nano Lett.* **2018**, *18*, 7991–7997.
- (40) Ozaki, N.; Sakamoto, H.; Nishihara, T.; Fujimori, T.; Hijikata, Y.; Kimura, R.; Irle, S.; Itami, K. Electrically Activated Conductivity and White Light Emission of a Hydrocarbon Nanoring–Iodine Assembly. *Angew. Chem., Int. Ed.* **2017**, *56*, 11196–11202.
- (41) Taber, B. N.; Gervasi, C. F.; Mills, J. M.; Kislitsyn, D. A.; Darzi, E. R.; Crowley, W. G.; Jasti, R.; Nazin, G. V. Quantum Confinement of Surface Electrons by Molecular Nanohoop Corrals. *J. Phys. Chem. Lett.* **2016**, *7*, 3073.
- (42) Tang, H.; Gu, Z.; Li, C.; Li, Z.; Wu, W.; Jiang, X. Nanoscale Vesicles Assembled from Non-Planar Cyclic Molecules for Efficient Cell Penetration. *Biomater. Sci.* **2019**, *7*, 2552–2558.
- (43) So, P. T.; Dong, C. Y.; Masters, B. R.; Berland, K. M. Two-Photon Excitation Fluorescence Microscopy. *Annu. Rev. Biomed. Eng.* **2000**, 2, 399–429.
- (44) de Reguardati, S.; Pahapill, J.; Mikhailov, A.; Stepanenko, Y.; Rebane, A. High-Accuracy Reference Standards for Two-Photon Absorption in the 680–1050 Nm Wavelength Range. *Opt. Express* **2016**, *24*, 9053.
- (45) Gao, P.; Pan, W.; Li, N.; Tang, B. Fluorescent Probes for Organelle-Targeted Bioactive Species Imaging. *Chem. Sci.* **2019**, *10*, 6035–6071.
- (46) Jasti, R.; Bhattacharjee, J.; Neaton, J. B.; Bertozzi, C. R. Synthesis, Characterization, and Theory of [9]-, [12]-, and [18]-Cycloparaphenylene: Carbon Nanohoop Structures. *J. Am. Chem. Soc.* **2008**, *130*, 17646–17647.
- (47) Suseela, Y. V.; Das, S.; Pati, S. K.; Govindaraju, T. Imidazolyl-Naphthalenediimide-Based Threading Intercalators of DNA. *Chem-BioChem* **2016**, *17*, 2162–2171.
- (48) Yang, N. J.; Hinner, M. J. Getting across the Cell Membrane: An Overview for Small Molecules, Peptides, and Proteins. *Methods Mol. Biol.* **2015**, *1266*, 29–53.
- (49) Wagner, J.; Li, L.; Simon, J.; Landfester, K.; Mailänder, V.; Müllen, K.; Ng, D. Y. W.; Wu, Y.; Weil, T.; Krutzke, L. Amphiphilic Polyphenylene Dendron Conjugates for Surface Remodeling of Adenovirus. *Angew. Chem., Int. Ed.* **2020**, *59*, 5712–11.
- (50) Stangenberg, R.; Wu, Y.; Hedrich, J.; Kurzbach, D.; Wehner, D.; Weidinger, G.; Kuan, S. L.; Jansen, M. I.; Jelezko, F.; Luhmann, H. J.; Hinderberger, D.; Weil, T.; Müllen, K. A Polyphenylene Dendrimer Drug Transporter with Precisely Positioned Amphiphilic Surface Patches. *Adv. Healthcare Mater.* **2015**, *4*, 377–384.
- (51) Lacerda, L.; Russier, J.; Pastorin, G.; Herrero, M. A.; Venturelli, E.; Dumortier, H.; Al-Jamal, K. T.; Prato, M.; Kostarelos, K.; Bianco, A. Translocation Mechanisms of Chemically Functionalised Carbon Nanotubes across Plasma Membranes. *Biomaterials* **2012**, *33*, 3334–3343.
- (52) Kaksonen, M.; Roux, A. Mechanisms of Clathrin-Mediated Endocytosis. *Nat. Rev. Mol. Cell Biol.* **2018**, *19*, 313–326.
- (53) Wu, L.; Li, X.; Ling, Y.; Huang, C.; Jia, N. Morpholine Derivative-Functionalized Carbon Dots-Based Fluorescent Probe for Highly Selective Lysosomal Imaging in Living Cells. *ACS Appl. Mater. Interfaces* **2017**, *9*, 28222–28232.
- (54) Kaufmann, A. M.; Krise, J. P. Niemann-Pick C1 Functions in Regulating Lysosomal Amine Content. *J. Biol. Chem.* **2008**, 283, 24584–24593.
- (55) Denk, W.; Strickler, J. H.; Webb, W. W. Two-Photon Laser Scanning Fluorescence Microscopy. *Science* **1990**, 248, 73–76.
- (56) Kim, H. M.; Cho, B. R. Small-Molecule Two-Photon Probes for Bioimaging Applications. *Chem. Rev.* **2015**, *115*, 5014–5055.
- (57) Xu, C.; Webb, W. W. Measurement of Two-Photon Excitation Cross Sections of Molecular Fluorophores with Data from 690 to 1050 Nm. *J. Opt. Soc. Am. B* **1996**, *13*, 481–491.

- (58) Mütze, J.; Iyer, V.; Macklin, J. J.; Colonell, J.; Karsh, B.; Petrášek, Z.; Schwille, P.; Looger, L. L.; Lavis, L. D.; Harris, T. D. Excitation Spectra and Brightness Optimization of Two-Photon Excited Probes. *Biophys. J.* **2012**, *102*, 934–944.
- Excitation Spectra and Brighness Optimization of Two-Fhoton Excited Probes. *Biophys. J.* **2012**, *102*, 934–944. (59) Pawlicki, M.; Collins, H. A.; Denning, R. G.; Anderson, H. L. Two-Photon Absorption and the Design of Two-Photon Dyes. *Angew. Chem., Int. Ed.* **2009**, *48*, 3244–3266.
- (60) Patterson, G. H.; Piston, D. W. Photobleaching in Two-Photon Excitation Microscopy. *Biophys. J.* **2000**, *78*, 2159–2162.